OPEN ACCESS Freely available online

PLOS ONE

Latrunculin A Treatment Prevents Abnormal Chromosome Segregation for Successful Development of Cloned Embryos

Yukari Terashita[1,2*], Kazuo Yamagata[1,3], Mikiko Tokoro[1,4], Fumiaki Itoi[1,4], Sayaka Wakayama[1,7], Chong Li[1,5], Eimei Sato[2,6], Kentaro Tanemura[2], Teruhiko Wakayama[1,7*]

1 Laboratory for Genomic Reprogramming, Center for Developmental Biology, RIKEN, Kobe, Japan, **2** Laboratory of Animal Reproduction, Graduate School of Agricultural Science, Tohoku University, Sendai, Japan, **3** Center for genetic analysis of biological responses, Research Institute for Microbial Diseases, Osaka University, Suita, Japan, **4** Asada Institute for Reproductive Medicine, Asada Ladies Clinic, Kasugai, Japan, **5** School of Medicine, Tongji University, Shanghai, China, **6** Managing director, National Livestock Breeding Center, Nishishirakawa-gun, Japan, **7** Department of Biotechnology, Faculty of Life and Environmental Science, University of Yamanashi, Kofu, Japan

Abstract

Somatic cell nuclear transfer to an enucleated oocyte is used for reprogramming somatic cells with the aim of achieving totipotency, but most cloned embryos die in the uterus after transfer. While modifying epigenetic states of cloned embryos can improve their development, the production rate of cloned embryos can also be enhanced by changing other factors. It has already been shown that abnormal chromosome segregation (ACS) is a major cause of the developmental failure of cloned embryos and that Latrunculin A (LatA), an actin polymerization inhibitor, improves F-actin formation and birth rate of cloned embryos. Since F-actin is important for chromosome congression in embryos, here we examined the relation between ACS and F-actin in cloned embryos. Using LatA treatment, the occurrence of ACS decreased significantly whereas cloned embryo-specific epigenetic abnormalities such as dimethylation of histone H3 at lysine 9 (H3K9me2) could not be corrected. In contrast, when H3K9me2 was normalized using the G9a histone methyltransferase inhibitor BIX-01294, the *Magea2* gene—essential for normal development but never before expressed in cloned embryos—was expressed. However, this did not increase the cloning success rate. Thus, non-epigenetic factors also play an important role in determining the efficiency of mouse cloning.

Citation: Terashita Y, Yamagata K, Tokoro M, Itoi F, Wakayama S, et al. (2013) Latrunculin A Treatment Prevents Abnormal Chromosome Segregation for Successful Development of Cloned Embryos. PLoS ONE 8(10): e78380. doi:10.1371/journal.pone.0078380

Editor: Zhongjun Zhou, The University of Hong Kong, Hong Kong

Received July 24, 2013; **Accepted** September 20, 2013; **Published** October 24, 2013

Funding: Financial support for this research was provided by Research Fellow of the Japan Society for the Promotion of Science to YT and Grant-in-Aid for Scientific Research on Priority Areas (20062015) and Scientific Research (A) (23248048) to TW. The funders had no role in study design, data collection and analysis, decision to publish, or preparation of the manuscript.

Competing interests: The authors have declared that no competing interests exist.

* E-mail: yterashita@cdb.riken.jp(YT); twakayama@yamanashi.ac.jp (TW)

Introduction

The oocyte's reprogramming ability to reset the genomic specialization of a somatic nucleus is the most efficient method used so far for cloning [1,2] and can give rise to full-term cloned animals [3,4]. Since cloned mice were first produced in 1998 [4], there have been many attempts at improving the birth rate [5], such as modifying the methodology [4,6], controlling the DNA acetylation status [7] and changing the timing of oocyte enucleation [8]. However, many disparities remained between normally fertilized embryos and cloned embryos and the birth rates of cloned embryos are still very low. The main cause of these problems is regarded as the incomplete reprogramming of the somatic epigenome and there have many studies aimed at improving the epigenetic status of cloned embryos [6,7,9-11]. However, some clone-specific epigenetic abnormalities, such as dimethylation of histone H3 at lysine 9 (H3K9me2), have never been corrected to the same level as in normally fertilized embryos by any treatment [12,13], whereas treatment with trichostatin A (TSA) improved the success rate of cloned mice by correcting other epigenetic abnormalities.

Here, we tried to improve the birth rate of cloned mice produced by somatic cell nuclear transfer (SCNT) in terms of alleviating both genetic and epigenetic problems in cloned embryos. For the epigenetic approach, we focused on H3K9me2, which serves as a binding region for heterochromatin protein 1 (HP1) [14,15]. HP1 localizes to

Journal of Reproduction and Development, Vol. 59, No 4, 2013

—Technology Report—

Selection of *In Vitro*-Matured Porcine Oocytes Based on Localization Patterns of Lipid Droplets to Evaluate Developmental Competence

Kou HIRAGA[1)], Yumi HOSHINO[1)], Kentaro TANEMURA[1)] and Eimei SATO[1)]

[1)]*Laboratory of Animal Reproduction, Graduate School of Agricultural Science, Tohoku University, Sendai 981-8555, Japan*

Abstract. Localization patterns of lipid droplets in the cytoplasm of porcine oocytes were evaluated as a novel marker for *in vitro* maturation (IVM) of oocytes with high developmental competence. Porcine oocytes were cultured in TCM-199, which is a complete synthetic medium, for 44 h at 38.5 C. Localization patterns were divided into 2 classes: lipid droplets localized uniformly in the whole cytoplasm (class I) and those that were centrally located (class II). After IVM in TCM-199, 60% of matured oocytes exhibited the class II pattern. To investigate the relation between the distribution of lipid droplets and the developmental rate of the oocyte, the developmental rates of class I and class II oocytes were compared after *in vitro* fertilization (IVF). Class II oocytes showed a significantly higher rate of blastocyst development than class I oocytes. These results suggest that porcine oocytes with high developmental competence can be selected based on the localization patterns of lipid droplets.
Key words: Lipid droplet, Novel marker, Porcine oocyte

(J. Reprod. Dev. 59: 405–408, 2013)

Porcine embryos from *in vitro* maturation (IVM) and *in vitro* fertilization (IVF) develop into blastocysts under *in vitro* conditions [1–3]; however, the developmental rates are very low compared with those of oocytes matured and fertilized *in vivo* [1, 3–6]. One factor contributing to this low developmental rate has been thought to be incomplete cytoplasmic maturation of the oocytes that mature *in vitro* [7]. Therefore, considerable improvement has been made to the IVM medium in which porcine oocytes are matured [7, 8]. A frequently used standard medium for IVM of porcine oocytes is North Carolina State University (NCSU)-23 [5] with porcine follicular fluid (pFF) supplementation [9–11]; however, follicular fluid contains numerous undefined factors and can be contaminated with viral pathogens [12–15]. Application of a fully defined IVM system eliminating follicular fluid from the medium could decrease the risk of viral contamination during *in vitro* production (IVP) of embryos. Tissue culture medium (TCM)-199, a complete synthetic medium for oocyte maturation, has been used in many laboratories [2, 16–18]. Blastocyst development [1, 2, 16, 17] and the birth of piglets [16] from oocytes matured in TCM-199 have been reported, although the efficiency has remained low.

To make the IVP system more stable for porcine oocytes using a complete synthetic medium, blastocyst production rate and quality had to be improved. Selection of IVM oocytes with high grades of cytoplasmic maturation for IVF would make further steps more easy by removing low-potential oocytes, saving time and materials and thus costs. Also, the quality of blastocysts, and developmental rate may improve. To do so, a simple, quick, and highly precise method for the evaluation of cytoplasmic maturity is needed. Using stereomicroscopic evaluation, immature oocytes appeared uniform in term of lipid droplet distribution in the cytoplasm (Fig. 1). We observed and classified the localization patterns of lipid droplets in matured oocytes after IVM in TCM-199 with stereomicroscope observation. In "class I" oocyte the lipid droplets were uniformly distributed throughout the entire cytoplasm, whereas in "class II" oocytes, the lipid droplets were centrally located in the cytoplasm (Fig. 2). As a result, significantly ($P<0.01$) more class II oocytes (% ± SEM = 60.9 ± 1.6) were observed after IVM than class I oocytes (27.3 ± 2.6). The remaining 11.8% of oocytes were degraded. The accuracy of classification of lipid droplet distribution by stereomicroscopy was verified by fluorescent lipid-specific staining (Fig. 2). To investigate the relationship between the distribution of lipid droplets and developmental rate, we compared developmental ability of class I and class II oocytes after IVF (Table 1). The blastocyst developmental rate of class II oocytes was significantly ($P<0.05$) higher than that of class I oocytes. However, cell number of the blastocyst was no different. That is, after IVM in TCM-199, the oocytes in which lipid droplets were centrally located had a higher developmental rate. The results suggest that the localization pattern of lipid droplets in porcine IVM oocytes can be an important indicator for selecting oocytes with high developmental competence.

The change in the localization of the cortical granules or mitochondria in IVM had previously been reported as a morphological marker of cytoplasmic maturation [19–21]. However, for such investigations, oocytes have to be fixed and dyed during evaluation, and they then cannot be used for *in vitro* fertilization and *in vitro* culture after IVM. The localization pattern of lipid droplets after IVM that became clear in our study is a morphological character that is observation without dye, enabling simple and quick evaluation of live oocytes. Evaluation of lipid droplet localization pattern in porcine IVM oocytes may also be a useful tool for clarifying the relationship between cytoplasmic maturation and developmental competence.

Sturmey and Leese reported that the level of triglycerides, which are main ingredients in lipid droplets in immature porcine oocytes decreased during IVM [22]. In addition, Somfai *et al.* reported that the

Received: August 29, 2012
Accepted: March 10, 2013
Published online in J-STAGE: April 18, 2013

Correspondence: K Hiraga (e-mail: b2ad1209@s.tohoku.ac.jp)

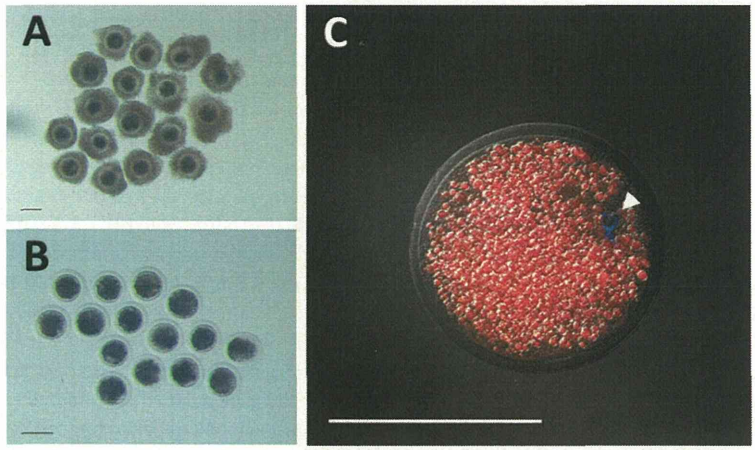

Fig. 1. Status of lipid droplets in porcine germinal vesicle (GV) oocytes. A: Selected COCs for IVM. B: Denuded GV oocyte. C: Immunostaining of lipid droplets. Intracellular lipids and DNA were stained by Nile red (red) and Hoechst 33342 (blue; arrowhead), respectively. Scale bar = 100 μm.

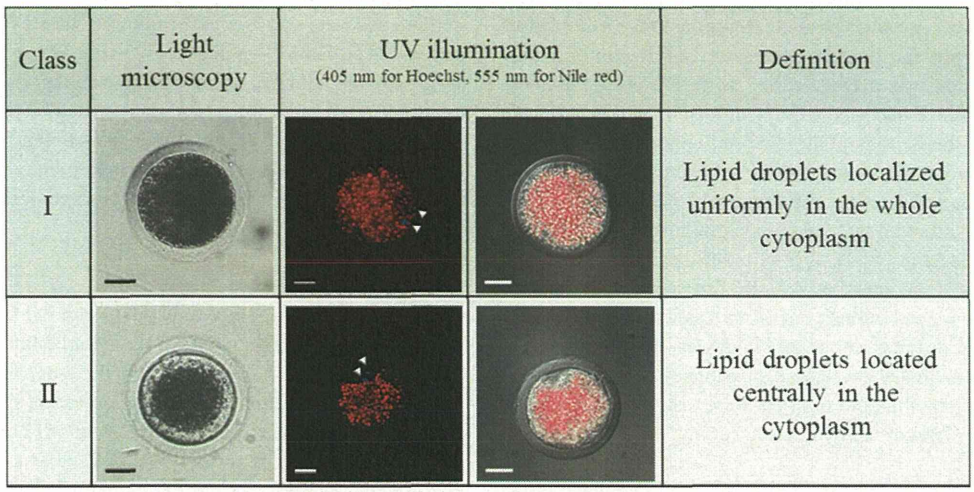

Fig. 2. Classification of localization patterns of lipid droplets in porcine oocytes after IVM. Intracellular lipids and DNA were stained by Nile red (red) and Hoechst 33342 (blue; arrowheads), respectively. Scale bar = 30 μm.

Table 1. Developmental competence of matured porcine oocytes with different localization patterns of lipid droplets

Lipid droplet distribution	No. of oocytes	Cleavage at Day 2 (%)	Blastocyst at Day 7 (%)	Cell number/ blastocyst
Class I	77	64 (85.3 ± 3.4)	3 (3.3 ± 2.1)[b]	48.7 ± 14.3
Class II	138	110 (80.6 ± 3.8)	23 (16.4 ± 3.6)[a]	50.6 ± 4.9

%: Mean ± SD. Day means day after fertilization. Different superscripts within columns indicate significant differences ($P<0.05$; 6 replicates).

addition of L-carnitine to the maturation medium, which enhances lipid metabolism, decreased intracellular lipids in porcine oocytes and improved maturation rate and division capability [23]. In accordance with these reports, our research suggests that lipid metabolism in porcine oocytes had an effect on cytoplasmic maturation in IVM and subsequent embryonic growth.

Methods

In vitro maturation

Ovaries were collected from prepubertal gilts at a local slaughterhouse and transported to the laboratory in a container within 2 h of

extraction. The follicular fluid and porcine oocytes were aspirated from antral follicles (diameter: 3–6 mm) by using a 10-ml syringe attached to an 18-gauge needle. Compact cumulus-oocyte complexes (COCs) with uniformly granulated cytoplasm were selected in PBS supplemented with 0.1% polyvinyl alcohol (PVA; Sigma, St. Louis, USA). After washing in 0.1% PBS-PVA, the COCs were cultured in TCM-199 supplemented with 2.2 mg/ml sodium bicarbonate (Sigma), 570 μM cysteamine (Sigma), 10 ng/ml EGF (Sigma), 100 mIU/ml FSH (Sigma), 100 IU/ml penicillin G (Gibco, Grand Island, USA), and 100 mg/ml streptomycin (Gibco). Groups of 25 oocytes were cultured in 250 μl of medium microdroplets for 44 h in an atmosphere containing 5% CO_2 at 38.5 C. Each droplet of medium was overlaid with liquid paraffin (Nacalai Tesque, Kyoto, Japan) in a 35-mm dish (Sumitomo Bakelite, Tokyo, Japan). At the end of culture, cumulus cells were removed from oocytes by glass micropipette after treatment with 0.1% hyaluronidase (Sigma) at room temperature.

Selection of lipid droplet localization patterns

After IVM, matured oocytes exposing the first polar body were selected under a stereomicroscope (Olympus, SZ-40, Tokyo, Japan) and used for subsequent experiments. Matured oocytes were observed with a stereomicroscope and classified according to the localization patterns of the lipid droplets. The standard classification of lipid droplet distribution was performed by using the public domain ImageJ program (developed at the U.S. National Institutes of Health and available on the Internet at http://rsb.info.nih.gov/ij). Matured oocytes were photographed using an inverted microscope (Olympus, IX70) and photography software (Olympus, DP2-BSW), and the pictures were transformed into 8-bit grayscale images. The area of the oocyte measured in the number of pixels, and the percentage of the total oocyte area occupied by lipid droplets was computed. An area showing a pixel intensity of 50 or less was assumed to be occupied by lipid droplets. In "class I" oocytes, the lipid droplets were uniformly distributed throughout the entire cytoplasm, whereas in "class II" oocytes, the lipid droplets were centrally located and covered less than 70% of the cytoplasm.

Evaluation of lipid droplets and chromosomes by confocal laser scanning microscopy

Oocytes were stained by the method of X-W Fu *et al.* with some modifications [24]. Denuded oocytes were fixed with 4% paraformaldehyde (Sigma) in phosphate-buffered saline (PBS) containing 0.1% polyvinyl alcohol (PBS-PVA) for at least 90 min at room temperature. The fixed oocytes were then rinsed three times in PBS-PVA, for 5 min each, and treated overnight with 10 μg/ml Nile red solution (Invitrogen, Grand Island, USA) dissolved in PBS-PVA at room temperature. The Nile red stock solution (1 mg/ml) was prepared by dilution in dimethyl sulfoxide (DMSO; Sigma) and stored at room temperature in the dark. Final concentrations were obtained by diluting the stock with saline solution. The following morning, they were briefly washed in PBS-PVA and stained with 5 μg/ml Hoechst 33342 (Sigma) in PBS-PVA for 20 min at room temperature. After being washed two additional times in PBS (5 min each), oocytes were mounted on nonfluorescent slides and observed under a confocal laser-scanning microscope (Zeiss LSM700, Oberkochen, Germany). Each treatment was repeated at least three times.

In vitro fertilization and culture

The methods for IVF and IVC were based on those described by Kikuchi *et al.* (2002) [11]. Epididymides from a Landrace boar were obtained, and epididymal spermatozoa were collected and frozen. Spermatozoa were thawed and preincubated for 30 min at 38.5 C in TCM-199 adjusted to pH 7.8. Fertilization medium (Pig-FM) for porcine oocytes consisting of 90 mM NaCl, 12 mM KCl, 25 mM $NaHCO_3$, 0.5 mM NaH_2PO_4, 0.5 mM $MgSO_4$, 10 mM sodium lactate (Kanto Chemical, Tokyo, Japan), and 10 mM HEPES was modified further by adding 8 mM CaCl2, 2 mM sodium pyruvate (Sigma), 2 mM caffeine, and 5 mg/ml BSA (Fraction V; Sigma). A portion (10 μl) of the preincubated spermatozoa was introduced into 90 μl of fertilization medium containing approximately 10 denuded oocytes. The final sperm concentration was adjusted to 1×10^5/ml. *In vitro* fertilization was carried out at 38.5 C under 5% CO_2. After IVF for 3 h, all putative zygotes were freed from the attached spermatozoa and transferred into IVC medium. The day of insemination was defined as day 0. The basic IVC medium was NCSU-37 containing 4 mg/ml BSA (Sigma) and 50 mM β-mercaptoethanol. Two types of IVC medium were prepared: 1) basic supplemented with 0.17 mM sodium pyruvate and 2.73 mM sodium lactate (IVC-PyrLac) and 2) basic with 5.55 mM D-glucose (IVC-Glu; Wako, Osaka, Japan), as originally reported [5]. Groups of 20 oocytes were cultured in 500 μl of IVC-PyrLac for 48 h, and then incubated in the IVC-Glu for an additional 120 h in an atmosphere containing 5% CO_2 at 38.5 C. Each droplet of medium was overlaid with liquid paraffin (Nacalai Tesque) in 4-well dishes (Nunc). These experiments were repeated at least five times.

Evaluation of embryo development

To examine their ability to develop into the blastocyst stage *in vitro*, all embryos and oocytes were cultured for 7 days, fixed and stained with 5 μg/ml Hoechst 33342 in PBS supplemented with 0.1% PVA; embryos were mounted on nonfluorescent slides and observed under a confocal laser-scanning microscope (Zeiss LSM700). An embryo with a clear blastocoel was defined as a blastocyst for the purposes of this study. The rate of blastocyst formation was evaluated, and the total number of cells in each blastocyst was evaluated as an indicator of embryo quality.

Statistical analysis

Statistical analyses were carried out using analysis of variance (ANOVA) and Fisher's protected least significant difference test using StatView. Differences of $P<0.05$ were considered significant.

Acknowledgments

We thank the staff of the Meat Inspection Office, Sendai City, Japan, for supplying the porcine ovaries. This work was supported by a Japan Society for the Promotion of Science grant to ES (No. 21248032).

References

1. **Nagashima H, Nagai T, Yamakawa H.** *In vitro* development of *in vivo* and *in vitro* fertilized pig zygotes. *J Reprod Dev* 1993; **2**: 163–168.
2. **Funahashi H, Cantley TC, Stumpf TT, Terlouw SL, Day BN.** *In vitro* development of *in vitro*-matured porcine oocytes following chemical activation or *in vitro* fertilization. *Biol Reprod* 1994; **50**: 1072–1077. [Medline]
3. **Rath D, Niemann H, Torres CR.** *In vitro* development to blastocysts of early porcine embryos produced *in vivo* or *in vitro*. *Theriogenology* 1995; **43**: 913–926. [Medline]
4. **Beckmann LS, Day BN.** Effects of media NaCl concentration and osmolarity on the culture of early-stage porcine embryos and the viability of embryos cultured in a selected superior medium. *Theriogenology* 1993; **39**: 611–622. [Medline]
5. **Petters RM, Wells KD.** Culture of pig embryos. *J Reprod Fertil Suppl* 1993; **48**: 61–73. [Medline]
6. **Dobrinsky JR, Johnson LA, Rath D.** Development of a culture medium (BECM-3) for porcine embryos: effects of bovine serum albumin and fetal bovine serum on embryo development. *Biol Reprod* 1996; **55**: 1069–1074. [Medline]
7. **Niwa K.** Effectiveness of *in vitro* maturation and *in vitro* fertilization techniques in pigs. *J Reprod Fertil Suppl* 1993; **48**: 49–59. [Medline]
8. **Nagai T.** *In vitro* maturation and fertilization of pig oocyte. *Anim Reprod Sci* 1996; **42**: 153–163.
9. **Funahashi H, Kim NH, Stumpf TT, Cantly TC, Day BN.** Presence of organic osmolytes in maturation medium enhances cytoplasmic maturation porcine oocyte. *Biol Reprod* 1996; **54**: 1412–1419. [Medline]
10. **Funahashi H, Cantley TC, Day BN.** Synchronization of meiosis in porcine oocytes by exposure to dibutyryl cyclic adenosine monophosphate improves developmental competence following *in vitro* fertilization. *Biol Reprod* 1997; **57**: 49–53. [Medline]
11. **Kikuchi K, Onishi A, Kashiwazaki N, Iwamoto M, Noguchi J, Kaneko H, Akita T, Nagai T.** Successful piglet production after transfer of blastocysts produced by a modified *in vitro* system. *Biol Reprod* 2002; **66**: 1033–1041. [Medline]
12. **Sur JH, Doster AR, Galeota JA, Osorio FA.** Evidence for the localization of porcine reproductive and respiratory syndrome virus (PRRSV) antigen and RNA in ovarian follicles in gilts. *Vet Pathol* 2001; **38**: 58–66. [Medline]
13. **Galik PK, Givens MD, Stringfellow DA, Crichton EG, Bishop MD, Eilertsen KJ.** Bovine viral diarrhea virus (BVDV) and anti-BVDV antibodies in pooled samples of follicular fluid. *Theriogenology* 2002; **57**: 1219–1227. [Medline]
14. **Devaux A, Soula V, Sifer C, Branger M, Naouri M, Porcher R, Poncelet C, Neuraz A, Alvarez S, Benifla JL, Madelenat P, Brun-Vazinet F, Feldmann G.** Hepatitis C virus detection in follicular fluid and culture media from HCV+ women, and viral risk during IVF procedures. *Hum Reprod* 2003; **18**: 2342–2349. [Medline]
15. **Pogranichniy R, Lee K, Machaty Z.** Detection of porcine parvovirus in the follicular fluid of abattoir pigs. *J Swine Health Prod* 2008; **16**: 244–246.
16. **Mattioli M, Bacci ML, Galeati G, Seren E.** Developmental competence of pig oocytes matured and fertilized *in vitro*. *Theriogenology* 1989; **31**: 1201–1207. [Medline]
17. **Yoshida M, Ishizaki Y, Kawagishi H.** Blastocyst formation by pig embryos resulting from *in-vitro* fertilization of oocytes matured *in vitro*. *J Reprod Fertil* 1990; **88**: 1–8. [Medline]
18. **Wang WH, Niwa K, Okuda K.** *In-vitro* penetration of pig oocytes matured in culture by frozen-thawed ejaculated spermatozoa. *J Reprod Fertil* 1991; **93**: 491–496. [Medline]
19. **Wang WH, Sun QY, Hosoe M, Shioya Y, Day BN.** Quantified analysis of cortical granule distribution and exocytosis of porcine oocytes during meiotic maturation and activation. *Biol Reprod* 1997; **56**: 1376–1382. [Medline]
20. **Sun QY, Wu GM, Lai L, Park KW, Cabot R, Cheong HT, Day BN, Prather RS, Schatten H.** Translocation of active mitochondria during pig oocyte maturation, fertilization and early embryo development *in vitro*. *Reproduction* 2001; **122**: 155–163. [Medline]
21. **Sha W, Xu BZ, Li M, Liu D, Feng HL, Sun QY.** Effect of gonadotropins on oocyte maturation *in vitro*: an animal model. *Fertil Steril* 2010; **93**: 1650–1661. [Medline]
22. **Sturmey RG, Leese HJ.** Energy metabolism in pig oocytes and early embryos. *Reproduction* 2003; **126**: 197–204. [Medline]
23. **Somfai T, Kaneda M, Akagi S, Watanabe S, Haraguchi S, Mizutani E, Dang-Nguyen TQ, Geshi M, Kikuchi K, Nagai T.** Enhancement of lipid metabolism with L-carnitine during *in vitro* maturation improves nuclear maturation and cleavage ability of follicular porcine oocytes. *Reprod Fertil Dev* 2011; **23**: 912–920. [Medline]
24. **Fu XW, Wu GQ, Li JJ, Hou YP, Zhou GB, Suo L, Wang YP, Zhu SE.** Positive effects of Forskolin (stimulator of lipolysis) treatment on cryosurvival of *in vitro* matured porcine oocytes. *Theriogenology* 2011; **75**: 268–275. [Medline]

heterochromatin domains [16] and is involved in downregulation of the *Magea* and *Xlr* family genes [10]. These genes have never been expressed in any cloned embryos even when genetically manipulated donor cells were used [6,10]. For the non-epigenetic approach, we focused on abnormal chromosome segregation (ACS). Although it is not clear whether ACS in cloned embryos is biologically or technically problem [17] and Balbach et al. reported that the karyotypes and chromosome segregation in cloned mouse embryos are not as bad either [18,19], at least some cloned embryos showed ACS and we recently reported that the birth rate of cloned mice could be improved by modifying the protocol rather than via epigenetic alteration [20]. Generally, reconstructed oocytes should be treated with actin polymerization inhibitors such as cytochalasin B (CB) or D during activation to keep all chromosomes inside the ooplasm, otherwise pseudo-second polar bodies can be extruded and some chromosomes derived from the donor nucleus will be lost [21]. Nevertheless, we found that F-actin localization in CB-treated cloned embryos was different from that seen in normally fertilized embryos. When we used latrunculin A (LatA)—a G-actin polymerization inhibitor —instead of CB, all chromosomes were kept inside the ooplasm without adverse effects on F-actin and the birth rate of cloned mice was increased [20]. Actin is an abundant protein present in all eukaryotic cells, and actin polymerization and depolymerization play fundamental roles in biological processes such as cell migration, determining cell shape, vesicle trafficking and regulating transcription [1,2,22,23]. It is also known that the F-actin meshwork that forms in the nuclear space is essential for preventing chromosome loss and aneuploidy in the embryo [24]. Such aneuploidy is one of the main causes of death in cloned embryos [25].

In the present study, we used live cell imaging to examine how LatA treatment affected the full-term development of cloned embryos not only in terms of epigenetic factors such as histone modifications and gene expression, but also for non-epigenetic factors such as chromosome segregation in early embryogenesis. In addition, we tried to correct H3K9me2 in cloned embryos using BIX-01294 (BIX) [26]. This is a specific inhibitor of the G9a histone methyltransferase responsible for dimethylation of H3K9 at transcriptionally silent regions [27,28]. However, this attempted correction of H3K9me2 did not improve the successful full-term development rate of cloned embryos.

Materials and Methods

Animals

B6D2F1 (C57BL/6 × DBA/2) strain female mice, aged 8–10 weeks, were used to produce oocytes. The surrogate pseudopregnant female mice used as embryo transfer recipients (see below) were ICR strain mice mated with vasectomized male mice of the same strain. B6D2F1 and ICR mice were purchased from Shizuoka Laboratory Animal Center (Hamamatsu, Japan). All animal experiments conformed to the Guide for the Care and Use of Laboratory Animals and were approved by the Institutional Committee of Laboratory Animal Experimentation of the RIKEN Center for Developmental Biology.

Collection of oocytes

Mature oocytes were collected from the oviducts of 8–10-week-old female mice that had been induced to superovulate with 5 IU pregnant mare serum gonadotropin (Teikokuzoki, Tokyo, Japan) followed by 5 IU human chorionic gonadotropin (hCG, Teikokuzoki) 48 h later. Cumulus-oocyte complexes (COCs) were collected from the oviducts approximately 16 h after hCG injection. After collection, COCs were placed in HEPES-buffered CZB medium (H-CZB) [29] and treated with 0.1% bovine testicular hyaluronidase (Sigma-Aldrich, St Louis, MO, USA). After several minutes, the cumulus-free oocytes were washed twice and then cultured in a droplet of potassium simplex optimized medium (KSOM) (Millipore [U.K.] Ltd., Watford, UK) at 37 °C under 5% CO_2 in air until used.

ICSI

Spermatozoa were collected from the cauda epididymidis of a mature B6D2F1 male mouse and incubated in H-CZB medium for more than 30 min at room temperature. ICSI was performed as described [30]. Briefly, the sperm head was separated from the tail by applying several piezo pulses to the neck region and the head was then injected into an oocyte. After 10 min of recovery at room temperature, the oocytes were cultured in KSOM as above until used for experiments.

In vitro fertilization

Cumulus-intact oocytes were collected in 0.2 ml of HTF medium [31] and inseminated with capacitated spermatozoa (final concentration 100/μl) [32]. After 2 h incubation at 37 °C under 5% CO_2 in air, the cumulus cells were dispersed by pipetting and cultured in KSOM as above for 96 h.

SCNT and embryo transfer

The SCNT procedure was performed as described [4]. Groups of oocytes were transferred into a droplet of H-CZB containing 5 μg/ml cytochalasin B (CB) for enucleation of the second meiotic division (MII) spindle. Oocytes undergoing microsurgery were held with a holding pipette and a hole was made in the zona pellucida following the application of several piezo pulses (Prime Tech, Ibaraki, Japan) to an enucleation pipette. The MII chromosome–spindle complex was aspirated into the pipette with a minimal volume of ooplasm. After enucleation of all oocytes, they were each injected with a cumulus cell nucleus. After nuclear transfer, the reconstructed oocytes were activated using 10 mM $SrCl_2$ in KSOM with 2 mM EGTA [33] in the presence of 5 μg/ml CB for 6 h or 5 μM LatA for 10 h. In both group, 50 nM TSA treatment was continued for 10 h [11]. Activation time of 10 h is longer than usual method, but full term development of cloned embryos was not affected by longer treatment of $SrCl_2$ [20]. In some experiments, 3 nM BIX was added together with TSA. Some cloned embryos were fixed for immunostaining and other cloned embryos were cultured in KSOM at 37 °C under 5% CO_2 after three washes in

KSOM. The preimplantation development rates of cloned embryos were examined from the PN to the blastocyst stages.

Embryo transfer and examination of placentae

To produce placenta in the LatA and CB experiments, ICSI-generated and cloned embryos at the 2-cell stage were transferred into the oviducts of pseudopregnant ICR females at 0.5 days postcoitus (dpc) and placentas were collected by caesarean section at 19.5 dpc. Placental weights were measured at the time of caesarean section and the placentas were fixed with 4% paraformaldehyde (PFA) for paraffin wax embedding and histology. The placentae were sectioned for staining with hematoxylin and eosin. In the BIX treatment experiments, cloned embryos at the morula stage were transferred into the uteri of pseudopregnant ICR females at 2.5 dpc and the live offspring were collected by caesarean section at 19.5 dpc.

Live cell imaging

Chromosomal dynamics during the first, second and third mitotic division of ICSI and cloned embryos were analyzed using live cell imaging technology. Messenger RNAs encoding EGFP–α-tubulin and mRFP–H2B were prepared as described [34]. Briefly, after linearization of the template plasmid at the Xba I site, mRNA was synthesized using the T7 RiboMAX™ Large Scale RNA Production System (Promega, Madison, WI, USA). The 5′ end of each mRNA was capped using Ribo m7G Cap Analog (Promega). To circumvent the integration of template DNA into the embryo genome, reaction mixtures from in vitro transcription runs were treated with RQ-1 RNase-free DNase I (Promega). Synthesized RNAs were treated with RQ-1 RNase-free DNase I (Promega). Synthesized RNAs were treated with phenol/chloroform followed by ethanol precipitation. After dissolution in RNase-free water, mRNAs were subjected to gel filtration using a MicroSpin™ G-25 column (Amersham Biosciences, Piscataway, NJ, USA) to remove unreacted substrates and then stored at -80 °C until used. Microinjection of mRNAs into oocytes was performed as described [35]. ICSI-generated or reconstructed oocytes were transferred to droplets of H-CZB medium in the observation chamber and a few picoliters of mRNA solution were introduced into the oocyte cytoplasm using a piezo-activated micromanipulator with a glass micropipette (1–3 μm diameter). The embryos were transferred to 5 μl drops of CZB medium on a glass-bottomed dish and placed in an incubation chamber set at 37 °C on the microscope stage. A gas mixture of 5% CO_2 and 95% air was introduced into the chamber. Fifty-one images in the z-axis and two color images were captured at 15 min intervals using a live cell imaging system [34]. Device control and image analysis were performed using MetaMorph software (Molecular Devices, Sunnyvale, CA, USA).

Immunostaining

Embryos at 10 h after activation were fixed in PBS containing 4% paraformaldehyde for 30 min. The fixed oocytes were washed twice in PBS containing 1% (w/v) BSA (Nacalai Tesque, Kyoto, Japan) (PBS-BSA) for 15 min each and then stored in PBS-BSA containing 0.1% (v/v) Triton X-100 (Nacalai Tesque) overnight at 4 °C. Embryos were then incubated with the primary antibodies: rabbit polyclonal anti-acH3K9 (1:100 dilution, Upstate Biotechnology Inc., Lake Placid, NY, USA), rabbit polyclonal anti-acH3K14 (1:100 dilution; Upstate Biotechnology Inc.), rabbit polyclonal anti-H3K9me2 (1:200 dilution; Millipore, Billerica, MA, USA), rabbit monoclonal anti-H3K4me2 (1:100 dilution; Abcam Japan, Tokyo, Japan) or goat polyclonal anti-heterochromatin protein (HP) 1α (1:100; Santa Cruz Biochemicals, Santa Cruz, CA, USA) and mouse monoclonal anti-H2B (1:400 dilution; Abcam Japan) in PBS-BSA overnight at 4 °C. After the embryos had been washed twice in PBS-BSA for 15 min each, they were incubated for 1 h with dye-conjugated secondary antibodies: Alexa-Fluor 488-labeled goat anti-mouse IgG (Molecular Probes Inc., Eugene, OR) and Alexa-Fluor 546-labeled goat anti-rabbit IgG (Molecular Probes Inc.). After the embryos had been washed twice in PBS-BSA, the DNA in embryos not stained with the anti-H2B antibody was stained with 2 μg/ml of DAPI (Molecular Probes Inc.). Then, after the embryos had been washed twice in PBS-BSA, serial images were taken using fluorescence confocal microscopy (FV-1000, Olympus Corp., Tokyo, Japan). Relative levels of acH3K9, acH3K14, H3K9me2, H3K4me2 and HP1α in embryos were measured using Olympus Fluor View (Olympus). Embryos were examined in PBS at 25 °C.

Real-time RT–PCR

Complementary DNA sequences from single ICSI-generated or cloned blastocysts were synthesized using Arcturus PicoPure RNA Isolation kits (Life Technologies, Carlsbad, CA, USA). Quantitative PCR was carried out on a StepOnePlus Real-Time RT–PCR system (Applied Biosystems, Foster City, CA, USA) using Fast SYBR Green Master Mix (Applied Biosystems). The *Gapdh* gene in each embryo was used for endogenous reference. The data on gene expression levels were analyzed using StepOnePlus software (Applied Biosystems). Primer sequences were as follows: 5′-gctccaactcctctgacctg-3′ and 5′-tgtccaatgagggtacagca-3′ for *Magea2*; 5′-agcagaattcaaggcaggag-3′ and 5′-gtccatctcaaccagccaat-3′ for *Xlr5c*; and 5′-ttcaccaccatggagaaggc-3′ and 5′-ccctttggctccaccct-3′ for *Gapdh*.

Statistical analysis

The incidence of ACS, blastocyst formation rates and offspring birth rates were evaluated using Chi-squared tests. Fluorescence levels, gene expression levels, and placental weights were analyzed by ANOVA followed by Fisher's protected least significant difference test; $P < 0.05$ was assumed to be statistically significant.

Results

Abnormal chromosomal segregation (ACS) during early embryogenesis

In a previous study, we reported that abnormal F-actin localization in cloned embryos was corrected by using LatA treatment [20]. Among many roles of F-actin in the cytoplasm,

here we focused on chromosomal segregation from the 1-cell to the 8-cell stage, which is critical for postimplantation development. Monomeric red fluorescent protein coupled with histone H2B (mRFP–H2B) and EGFP-tagged α-tubulin were expressed in embryos by mRNA injection immediately after SCNT or intracytoplasmic sperm injection (ICSI) and chromosomal segregation was monitored. Some embryos at these stages showed abnormal chromosomal behavior in mitotic blastomeres. Parts of the chromosomes were misaligned with the metaphase plate and lagging chromosomes were found at anaphase (Figure 1A). Consequently, ectopic micronuclei appeared as a result of ACS (Figure 1B-D). The incidence of ACS in cloned embryos produced with CB treatment was significantly higher than in ICSI-generated control embryos at the first, second and third cell division. However, when using LatA instead of CB, the incidence of ACS decreased significantly at the 2-cell stage and became similar to control embryos at the 4-cell and 8-cell stages (Figure 1E).

Epigenetic abnormalities in cloned embryos produced with CB or LatA

Our next question was whether the increased success rate of cloned mice produced by LatA treatment arose from modifications of epigenetic abnormalities. To investigate this, CB- or LatA-treated cloned embryos and ICSI-generated embryos were fixed at the pronuclear stage and immunostained with antibodies to acetylated histone H3 at lysines 9 or 14 (acH3K9 or acH3K14, respectively), to H3K9me2, to dimethylated histone H3 at lysine 14 (H3K14me2) and to H2B. As shown in Figure 2, the acetylation or methylation levels were not different between CB- and LatA-treated cloned embryos, but were abnormally high or low, respectively, compared with control embryos.

Epigenetic abnormalities in cloned placentae produced with CB or LatA treatments

It is well known that most cloned animals possess abnormal placentae arising from epigenetic errors [36-38]. Placentae derived from cloned or ICSI-generated control embryos were collected at embryonic day (E)19.5 and their weights and histology were compared. Abnormally heavy placentae and the abnormal distortion of the boundary between spongiotrophoblast and labyrinth layers were not corrected with LatA treatment (Figure 3).

Effect of BIX-01294 on cloned preimplantation embryos

H3K9me2 plays an important role in gene silencing but so far no cloning method has been able to correct abnormally high H3K9me levels in cloned embryos. We tried to control the H3K9me2 status in cloned embryos by using BIX, a specific inhibitor of the G9a histone methyltransferase. First, we examined the maximum concentration of BIX that did not decrease the blastocyst formation rate in control embryos and decided to use 3 nM, which led to the highest blastocyst formation rate. (Figure 4A). Then we examined the effect of this treatment on cloned embryos in terms of G9a target gene expression and H3K9me2 level. Real-time RT–PCR was performed at the blastocyst stage using ICSI-generated, control cloned embryos and BIX-treated cloned embryos. As shown in Figure 4B, *Magea2* gene expression was significantly upregulated by BIX treatment ($P < 0.05$). This result is consistent with the report that *Magea2* expression in ES cells is controlled by G9a through H3K9me2 at the promoter site [26]. When 1-cell stage cloned embryos were examined by immunostaining, BIX treatment decreased the H3K9me2, HP1α and acH3K9 levels significantly (Figure 4C–F; $P < 0.05$).

Effects of BIX on full-term development of cloned embryos

Finally, we examined whether correcting the epigenetic abnormalities at H3K9me2 in cloned embryos could lead to full-term development. Although BIX treatment reduced the level of H3K9me2 in cloned preimplantation embryos, the birth rate of cloned mice following BIX treatment was 7.8% (8/102), almost the same as untreated controls (7.3%, 9/123; Table 1). Thus, alleviating this particular epigenetic aberration in cloned embryos did not improve development to term.

Discussion

Previously, we reported that LatA treatment corrected aberrant F-actin localization in cloned embryos and increased the birth rate of cloned mice [20]. However, the association between inhibition of actin polymerization at the 1-cell stage and full-term development was not clear. F-actin in the nucleus has an important role in chromosome transport [24] and cloned embryos exhibiting ACS before the 8-cell stage cannot develop to full term [25]. We confirmed here that the occurrence of ACS was significantly higher than controls in CB-treated cloned embryos at the 2-cell stage, but this decreased significantly to the same level as ICSI-generated embryos when using LatA instead of CB. Thus, LatA appears to improve the birth rate associated with ACS in cloned embryos by gently inhibiting actin polymerization; importantly, this event was not linked directly to epigenetic alterations. When specific histone modifications associated with either active (acH3K9 and H3K4me2) or repressed (H3K9me2) chromatin, and with aberrant spindles in oocytes (acH3K14) [27,28] were examined, these were not improved by using LatA instead of CB.

Next, we focused on the H3K9me2 abnormality in cloned embryos because its level decreases quickly in normally fertilized embryos to allow the proper expression of several genes but persists in cloned embryos [6,12,13,39-42]. This methylated histone region serves as a binding platform for HP1 [14,15,43]; correspondingly, HP1 expression was significantly higher in cloned embryos than in zygotes fertilized in vitro [44]. In addition, H3K9-related genes, such as *Magea* and *Xlr*, also failed to be expressed in cloned embryos even when the expression of *Xist* was controlled [10].

In this study, we used BIX as a specific inhibitor of G9a [27]. The H3K9me2 level at the *Magea2* promoter region was decreased by BIX treatment [26]. Consistent with this result, when we treated cloned embryos with BIX, H3K9me2 and HP1α levels were significantly decreased and *Magea2* gene

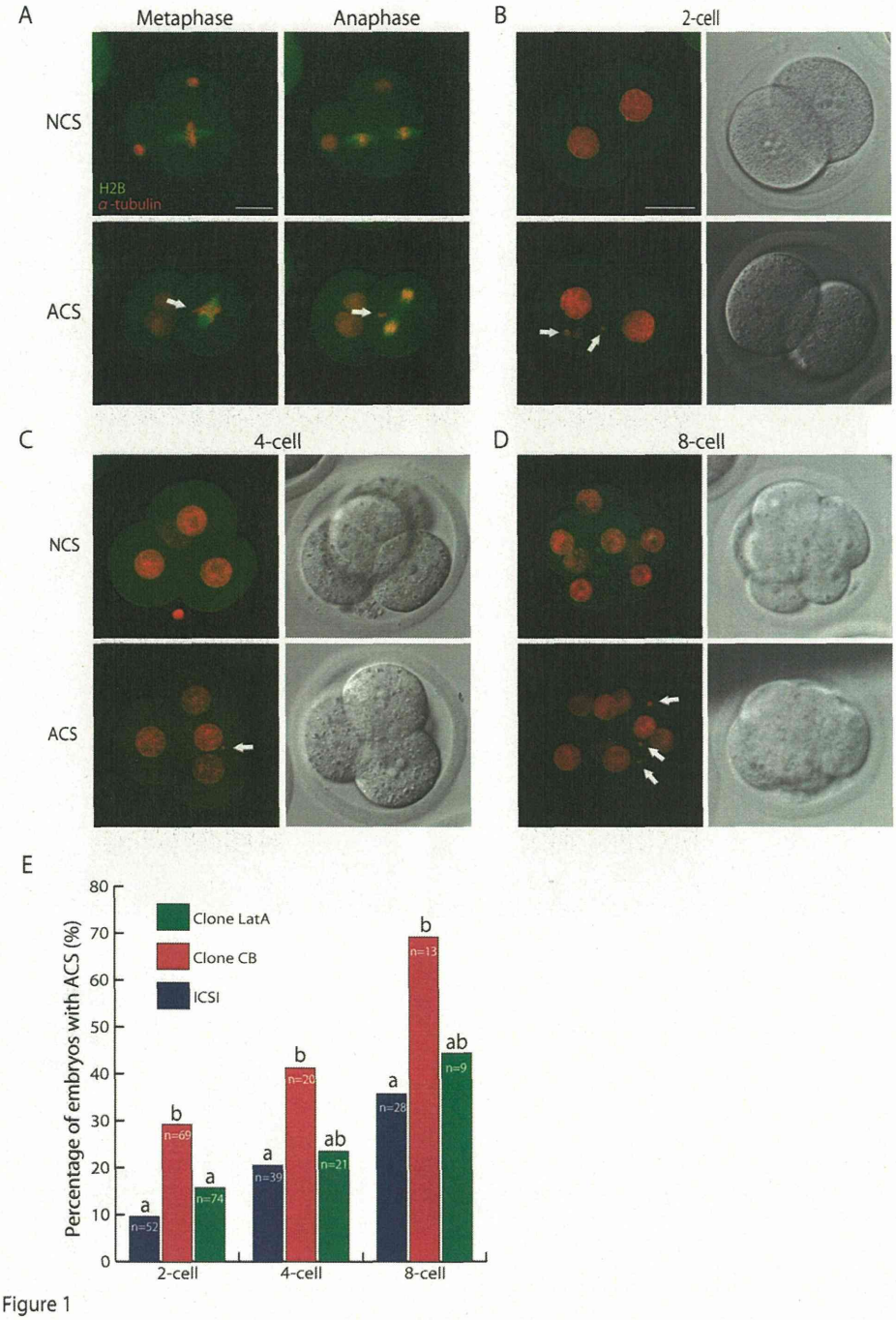

Figure 1

Figure 1. Chromosome segregation in early embryonic development. (A) Chromosomes were misaligned at metaphase and lagging chromosomes were found at anaphase in embryos ACS was occured. (B-D) Merged and bright field images of embryos with normal chromosomal segregation (NCS) and abnormal chromosomal segregation (ACS). As an example, time-lapse images of chromosome segregation at the first, second and third mitosis are shown at the 2-cell, 4-cell and 8-cell stages, respectively. Arrows indicate chromosomal fragments appearing during the division. Green, EGFP-α-tubulin; red, mRFP–H2B. Bar = 30 μm. (E) The percentages of embryos with ACS at the 2-cell, 4-cell and 8-cell stages in ICSI-generated and cloned embryos. Values with different superscripts in the same category differ significantly between ICSI-generated, CB- and LatA-treated cloned embryos.

doi: 10.1371/journal.pone.0078380.g001

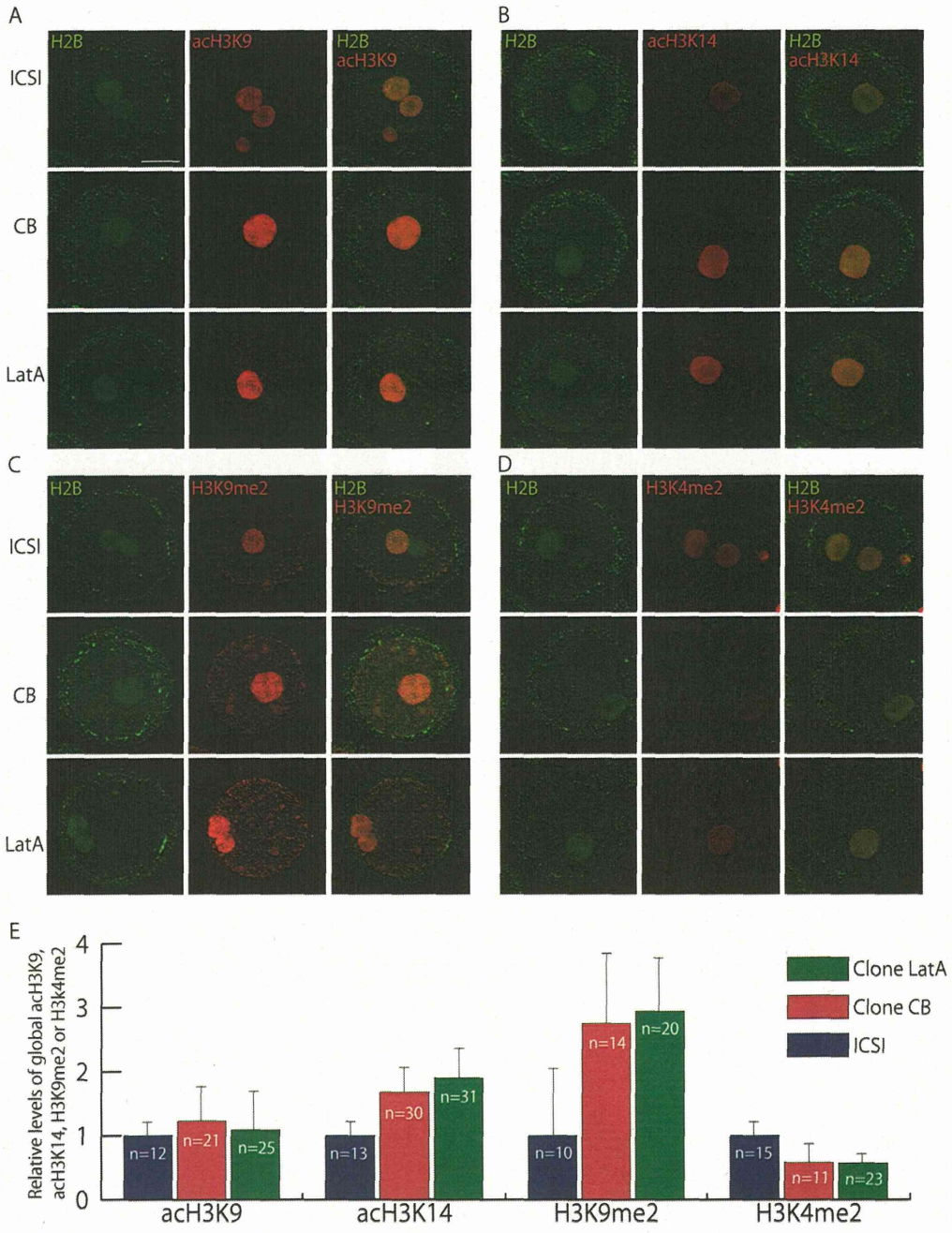

Figure 2

Figure 2. Histone modifications in 1-cell stage embryos. (A-D) acH3K9, acH3K14, H3K9me2 or H3K4me2 levels in ICSI-generated and CB- or LatA-treated cloned embryos. Bar = 30 μm. (E) The intensities of immunofluorescence for acH3K9, acH3K14, H3K9me2 and H3K4me2 relative to that of H2B. They are compared with the intensities in ICSI-generated control embryos. The acetylation or methylation levels of these regions were not different between LatA- and CB-treated cloned embryos.

doi: 10.1371/journal.pone.0078380.g002

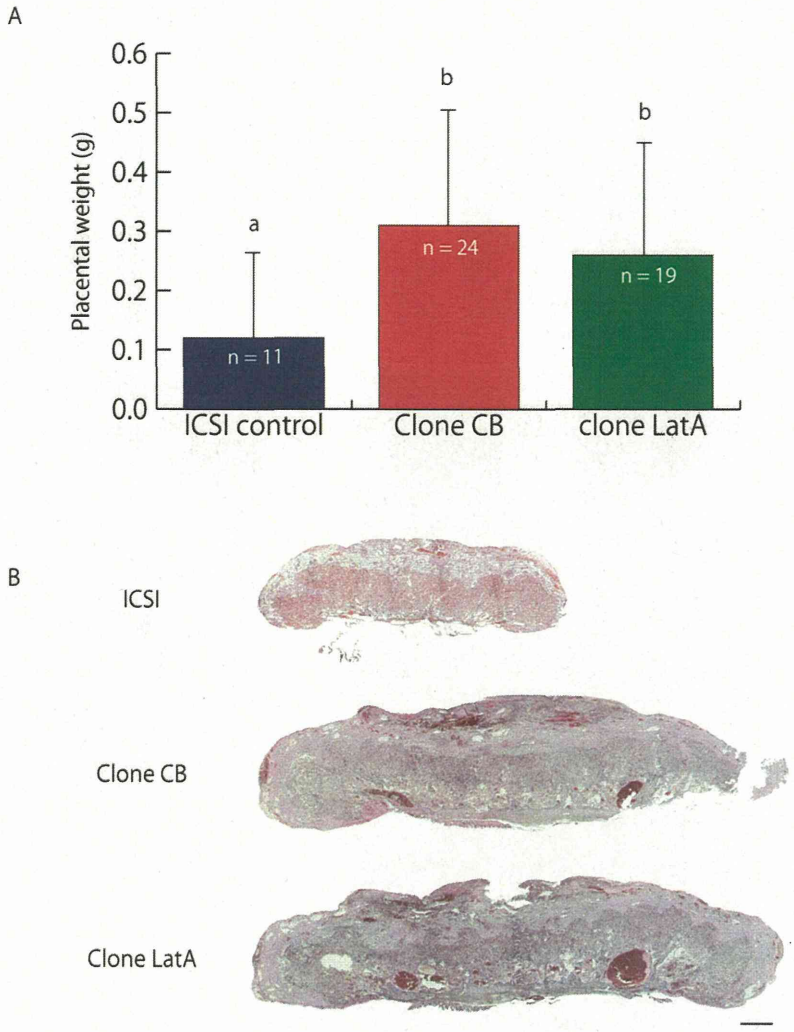

Figure 3

Figure 3. Abnormalities in placentae derived from cloned embryos. (A) Placental weights from ICSI-derived control embryos and CB- or LatA-treated cloned embryos. Error bars indicate SD. Asterisks indicate significant difference at $p < 0.05$. (B) Hematoxylin and eosin staining of placentae derived from ICSI-derived control and CB- or LatA-treated cloned embryos. Abnormal distortion of the boundary between the spongiotrophoblast and labyrinth layers was observed in placentas derived from both CB- and LatA-treated cloned embryos. Bar = 500 μm.

doi: 10.1371/journal.pone.0078380.g003

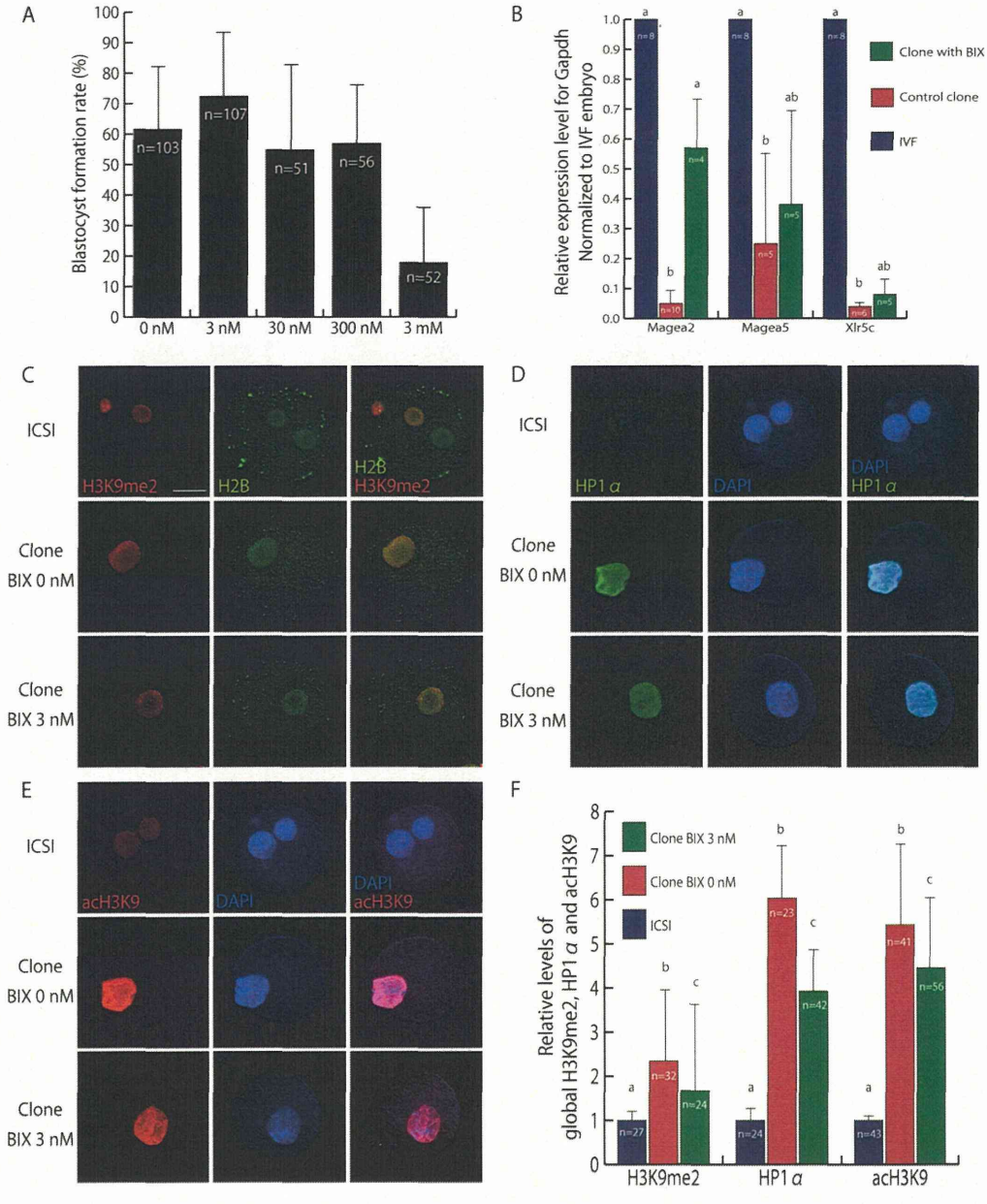

Figure 4

Figure 4. The effect of BIX on cloned embryos. (A) Blastocyst formation rate of cloned embryos treated with various concentrations of BIX. (B) Relative expression level of *Magea* and *Xlr* family genes in a blastocyst. The level of mRNA was normalized to the *Gapdh* expression level in the same sample. These genes were strongly repressed in control cloned blastocysts, but the reduced *Magea2* expression was increased by treatment with BIX. (C–F) Fluorescence level of H3K9me2, HP1α and acH3K9 normalized to the DAPI or histone H2B level of the same sample. Bar = 30 μm. BIX treatment was effective in decreasing H3K9me2, HP1α and acH3K9 levels.

doi: 10.1371/journal.pone.0078380.g004

Table 1. The effect of BIX on full term development of cloned embryos.

Treatment	No. reconstructed oocytes	No. survived after activation	No. PN formed	No. 2-cell embryos (%/PN)	No. morulae (%/PN)	No. embryos transferred (recipients)	No. live offspring (%/ET)	Mean body weight (g)	Mean placental weight (g)
Control	239	178	160	146 (91.3)	123 (76.9)	123 (13)	9 (7.3)	1.80 ± 0.24	0.30 ± 0.09
BIX 3 nM	194	152	140	125 (89.3)	102 (72.9)	102 (8)	8 (7.8)	2.12 ± 0.43	0.33 ± 0.04

PN, pronuclei; ET, embryo transfer

doi: 10.1371/journal.pone.0078380.t001

expression was improved, while the expression levels of *Magea5* and *Xlr5c* were not increased significantly. However, the birth rate of cloned mice was not increased at all. Surprisingly, the acH3K9 level decreased, so several other H3K9me-related genes might remain silenced in BIX-treated cloned embryos and thereby lead to embryo death. Because Xist knockout or knockdown did not change the expression patterns of *Magea* and *Xlr* family genes in cloned embryos [6,10], H3K9me2 might be a reprogramming-resistant region of the SCNT nucleus, and other approaches targeting these sites might be needed for proper genomic reprogramming.

In conclusion, while BIX treatment did not increase the birth rate of cloned mice even though some epigenetic errors were corrected to some extent, LatA treatment promoted normal chromosome segregation in the context of proper F-actin formation and improved the full-term development of cloned embryos with epigenetic abnormalities remained. Thus, non-epigenetic factors, such as F-actin formation and chromosome segregation in early stage of preimplantation embryos, also play an important role in determining the success rate of mouse cloning.

Acknowledgements

We are grateful to the Laboratory for Animal Resources and Genetic Engineering for housing the mice.

Author Contributions

Conceived and designed the experiments: YT KY TW. Performed the experiments: YT MT FI. Analyzed the data: YT. Contributed reagents/materials/analysis tools: YT SW CL. Wrote the manuscript: YT TW. Supported doing experiments and writing the manuscript: ES KT.

References

1. Jullien J, Pasque V, Halley-Stott RP, Miyamoto K, Gurdon JB (2011) Mechanisms of nuclear reprogramming by eggs and oocytes: a deterministic process? Nat Rev Mol Cell Biol 12: 453-459. doi:10.1038/nrg3034. PubMed: 21697902.
2. Kim K, Doi A, Wen B, Ng K, Zhao R et al. (2010) Epigenetic memory in induced pluripotent stem cells. Nature 467: 285-290. doi:10.1038/nature09342. PubMed: 20644535.
3. Wilmut I, Schnieke AE, McWhir J, Kind AJ, Campbell KH (1997) Viable offspring derived from fetal and adult mammalian cells. Nature 385: 810-813. doi:10.1038/385810a0. PubMed: 9039911.
4. Wakayama T, Perry AC, Zuccotti M, Johnson KR, Yanagimachi R (1998) Full-term development of mice from enucleated oocytes injected with cumulus cell nuclei. Nature 394: 369-374. doi:10.1038/28615. PubMed: 9690471.
5. Thuan NV, Kishigami S, Wakayama T (2010) How to improve the success rate of mouse cloning technology. J Reprod Dev 56: 20-30. doi:10.1262/jrd.09-221A. PubMed: 20203432.
6. Inoue K, Kohda T, Sugimoto M, Sado T, Ogonuki N et al. (2010) Impeding Xist Expression from the Active X Chromosome Improves Mouse Somatic Cell Nuclear Transfer. Science, 330: 496–9. PubMed: 20847234.
7. Ono T, Li C, Mizutani E, Terashita Y, Yamagata K et al. (2010) Inhibition of class IIb histone deacetylase significantly improves cloning efficiency in mice. Biol Reprod 83: 929-937. doi:10.1095/biolreprod.110.085282. PubMed: 20686182.
8. Wakayama S, Cibelli JB, Wakayama T (2003) Effect of timing of the removal of oocyte chromosomes before or after injection of somatic nucleus on development of NT embryos. Cloning Stem Cells 5: 181-189. doi:10.1089/153623003769645848. PubMed: 14588136.
9. Ogura A, Inoue K, Wakayama T (2013) Recent advancements in cloning by somatic cell nuclear transfer. Philos Trans R Soc Lond B Biol Sci 368: 20110329. PubMed: 23166393.
10. Matoba S, Inoue K, Kohda T, Sugimoto M, Mizutani E et al. (2011) RNAi-mediated knockdown of Xist can rescue the impaired postimplantation development of cloned mouse embryos. Proc Natl Acad Sci U S A 108: 20621-20626. doi:10.1073/pnas.1112664108. PubMed: 22065773.
11. Kishigami S, Mizutani E, Ohta H, Hikichi T, Thuan NV et al. (2006) Significant improvement of mouse cloning technique by treatment with trichostatin A after somatic nuclear transfer. Biochem Biophys Res Commun 340: 183-189. doi:10.1016/j.bbrc.2005.11.164. PubMed: 16356478.
12. Wang F, Kou Z, Zhang Y, Gao S (2007) Dynamic reprogramming of histone acetylation and methylation in the first cell cycle of cloned mouse embryos. Biol Reprod 77: 1007-1016. doi:10.1095/biolreprod.107.063149. PubMed: 17823087.
13. Bui HT, Wakayama S, Kishigami S, Park KK, Kim JH et al. (2010) Effect of trichostatin A on chromatin remodeling, histone modifications, DNA replication, and transcriptional activity in cloned mouse embryos. Biol Reprod 83: 454-463. doi:10.1095/biolreprod.109.083337. PubMed: 20505166.
14. Bannister AJ, Zegerman P, Partridge JF, Miska EA, Thomas JO et al. (2001) Selective recognition of methylated lysine 9 on histone H3 by the HP1 chromo domain. Nature 410: 120-124. doi:10.1038/35065138. PubMed: 11242054.
15. Lachner M, O'Carroll D, Rea S, Mechtler K, Jenuwein T (2001) Methylation of histone H3 lysine 9 creates a binding site for HP1 proteins. Nature 410: 116-120. doi:10.1038/35065132. PubMed: 11242053.
16. Smothers JF, Henikoff S (2001) The hinge and chromo shadow domain impart distinct targeting of HP1-like proteins. Mol Cell Biol 21: 2555-2569. doi:10.1128/MCB.21.7.2555-2569.2001. PubMed: 11259603.
17. Yu Y, Ding C, Wang E, Chen X, Li X et al. (2007) Piezo-assisted nuclear transfer affects cloning efficiency and may cause apoptosis. Reproduction 133: 947-954. doi:10.1530/REP-06-0358. PubMed: 17616724.
18. Balbach ST, Jauch A, Böhm-Steuer B, Cavaleri FM, Han YM et al. (2007) Chromosome stability differs in cloned mouse embryos and derivative ES cells. Dev Biol 308: 309-321. doi:10.1016/j.ydbio.2007.05.034. PubMed: 17610862.

19. Balbach ST, Esteves TC, Houghton FD, Siatkowski M, Pfeiffer MJ et al. (2012) Nuclear reprogramming: kinetics of cell cycle and metabolic progression as determinants of success. PLOS ONE 7: e35322. doi: 10.1371/journal.pone.0035322. PubMed: 22530006.
20. Terashita Y, Wakayama S, Yamagata K, Li C, Sato E et al. (2012) Latrunculin a can improve the birth rate of cloned mice and simplify the nuclear transfer protocol by gently inhibiting actin polymerization. Biol Reprod 86: 180. doi:10.1095/biolreprod.111.098764. PubMed: 22492972.
21. Wakayama T, Yanagimachi R (2001) Effect of cytokinesis inhibitors, DMSO and the timing of oocyte activation on mouse cloning using cumulus cell nuclei. Reproduction 122: 49-60. doi:10.1530/rep.0.1220049. PubMed: 11425329.
22. Miyamoto K, Gurdon JB (2012) Transcriptional regulation and nuclear reprogramming: roles of nuclear actin and actin-binding proteins. Cell Mol Life Sci, 70: 3289–302. PubMed: 23275942.
23. Miyamoto K, Pasque V, Jullien J, Gurdon JB (2011) Nuclear actin polymerization is required for transcriptional reprogramming of Oct4 by oocytes. Genes Dev 25: 946-958. doi:10.1101/gad.615211. PubMed: 21536734.
24. Mori M, Monnier N, Daigle N, Bathe M, Ellenberg J et al. (2011) Intracellular transport by an anchored homogeneously contracting F-actin meshwork. Curr Biol 21: 606-611. doi:10.1016/j.cub.2011.03.002. PubMed: 21439825.
25. Mizutani E, Yamagata K, Ono T, Akagi S, Geshi M et al. (2012) Abnormal chromosome segregation at early cleavage is a major cause of the full-term developmental failure of mouse clones. Dev Biol 364: 56-65. doi:10.1016/j.ydbio.2012.01.001. PubMed: 22266425.
26. Kubicek S, O'Sullivan RJ, August EM, Hickey ER, Zhang Q et al. (2007) Reversal of H3K9me2 by a small-molecule inhibitor for the G9a histone methyltransferase. Mol Cell 25: 473-481. doi:10.1016/j.molcel.2007.01.017. PubMed: 17289593.
27. Tachibana M, Sugimoto K, Nozaki M, Ueda J, Ohta T et al. (2002) G9a histone methyltransferase plays a dominant role in euchromatic histone H3 lysine 9 methylation and is essential for early embryogenesis. Genes Dev 16: 1779-1791. doi:10.1101/gad.989402. PubMed: 12130538.
28. Rice JC, Briggs SD, Ueberheide B, Barber CM, Shabanowitz J et al. (2003) Histone methyltransferases direct different degrees of methylation to define distinct chromatin domains. Mol Cell 12: 1591-1598. doi:10.1016/S1097-2765(03)00479-9. PubMed: 14690610.
29. Chatot CL, Lewis JL, Torres I, Ziomek CA (1990) Development of 1-cell embryos from different strains of mice in CZB medium. Biol Reprod 42: 432-440. doi:10.1095/biolreprod42.3.432. PubMed: 2111184.
30. Kimura Y, Yanagimachi R (1995) Intracytoplasmic sperm injection in the mouse. Biol Reprod 52: 709-720. doi:10.1095/biolreprod52.4.709. PubMed: 7779992.
31. Nakagata N (1996) Use of cryopreservation techniques of embryos and spermatozoa for production of transgenic (Tg) mice and for maintenance of Tg mouse lines. Lab Anim Sci 46: 236-238. PubMed: 8723247.
32. Yamagata K, Suetsugu R, Wakayama T (2009) Assessment of chromosomal integrity using a novel live-cell imaging technique in mouse embryos produced by intracytoplasmic sperm injection. Hum Reprod 24: 2490-2499. doi:10.1093/humrep/dep236. PubMed: 19574276.
33. Kishigami S, Wakayama T (2007) Efficient strontium-induced activation of mouse oocytes in standard culture media by chelating calcium. J Reprod Dev 53: 1207-1215. doi:10.1262/jrd.19067. PubMed: 17938555.
34. Yamagata K, Suetsugu R, Wakayama T (2009) Long-term, six-dimensional live-cell imaging for the mouse preimplantation embryo that does not affect full-term development. J Reprod Dev 55: 343-350. doi:10.1262/jrd.20166. PubMed: 19305125.
35. Yamagata K (2010) DNA methylation profiling using live-cell imaging. Methods 52: 259-266. doi:10.1016/j.ymeth.2010.04.008. PubMed: 20412856.
36. Tanaka S, Oda M, Toyoshima Y, Wakayama T, Tanaka M et al. (2001) Placentomegaly in cloned mouse concepti caused by expansion of the spongiotrophoblast layer. Biol Reprod 65: 1813-1821. doi:10.1095/biolreprod65.6.1813. PubMed: 11717146.
37. Ohgane J, Wakayama T, Kogo Y, Senda S, Hattori N et al. (2001) DNA methylation variation in cloned mice. Genesis 30: 45-50. doi:10.1002/gene.1031. PubMed: 11416862.
38. Inoue K, Kohda T, Lee J, Ogonuki N, Mochida K et al. (2002) Faithful expression of imprinted genes in cloned mice. Science 295: 297. doi: 10.1126/science.295.5553.297. PubMed: 11786635.
39. Ohgane J, Wakayama T, Senda S, Yamazaki Y, Inoue K et al. (2004) The Sall3 locus is an epigenetic hotspot of aberrant DNA methylation associated with placentomegaly of cloned mice. Genes Cells 9: 253-260. doi:10.1111/j.1356-9597.2004.00720.x. PubMed: 15005712.
40. Kang YK, Koo DB, Park JS, Choi YH, Chung AS et al. (2001) Aberrant methylation of donor genome in cloned bovine embryos. Nat Genet 28: 173-177. doi:10.1038/88903. PubMed: 11381267.
41. Dean W, Santos F, Stojkovic M, Zakhartchenko V, Walter J et al. (2001) Conservation of methylation reprogramming in mammalian development: aberrant reprogramming in cloned embryos. Proc Natl Acad Sci U S A 98: 13734-13738. doi:10.1073/pnas.241522698. PubMed: 11717434.
42. Santos F, Zakhartchenko V, Stojkovic M, Peters A, Jenuwein T et al. (2003) Epigenetic marking correlates with developmental potential in cloned bovine preimplantation embryos. Curr Biol 13: 1116-1121. doi: 10.1016/S0960-9822(03)00419-6. PubMed: 12842010.
43. Epsztejn-Litman S, Feldman N, Abu-Remaileh M, Shufaro Y, Gerson A et al. (2008) De novo DNA methylation promoted by G9a prevents reprogramming of embryonically silenced genes. Nat Struct Mol Biol 15: 1176-1183. doi:10.1038/nsmb.1476. PubMed: 18953337.
44. Nowak-Imialek M, Wrenzycki C, Herrmann D, Lucas-Hahn A, Lagutina I et al. (2008) Messenger RNA expression patterns of histone-associated genes in bovine preimplantation embryos derived from different origins. Mol Reprod Dev 75: 731-743. doi:10.1002/mrd.20816. PubMed: 18058811.

RESEARCH ARTICLE

Molecular Reproduction & Development 80:334–348 (2013)

Distribution and Association of mTOR With Its Cofactors, Raptor and Rictor, in Cumulus Cells and Oocytes During Meiotic Maturation in Mice

YUHEI KOGASAKA,* YUMI HOSHINO, YUUKI HIRADATE, KENTARO TANEMURA, AND EIMEI SATO

Laboratory of Animal Reproduction, Graduate School of Agricultural Science, Tohoku University, Sendai, Japan

SUMMARY

Mammalian target of rapamycin (mTOR), a Ser/Thr protein kinase, is the catalytic component of two distinct signaling complexes, mTOR-raptor complex (mTORC1) and mTOR-rictor complex (mTORC2). Recently, studies have demonstrated mitosis-specific roles for mTORC1, but the functions and expression dynamics of mTOR complexes during meiotic maturation remain unclear. In the present study, to evaluate the roles of respective mTOR complexes in maternal meiosis and compare them with those in mitosis, we sought to elucidate the spatiotemporal immunolocalization of mTOR, the kinase-active Ser2448- and Ser2481-phosphorylated mTOR, and raptor and rictor during cumulus-cell mitosis and oocyte meiotic maturation in mice. mTOR principally accumulated around the chromosomes and on the spindle. Phosphorylated mTOR (Ser2448 and Ser2481) exhibited elevated fluorescence intensities in the cytoplasm and punctate localization adjacent to the chromosomes, on the spindle poles, and on the midbody during mitotic and meiotic maturation, suggesting functional homology of mTOR between the two cell division systems, despite their mechanistically distinctive spindles. Raptor colocalized with mTOR during both types of cell division, indicating that mTORC1 is predominantly associated with these events. Mitotic rictor uniformly distributed through the cytoplasm, and meiotic rictor localized around the spindle poles of metaphase-I oocytes, suggesting functional divergence of mTORC2 between mitosis and female meiosis. Based on the general function of mTORC2 in the organization of the actin cytoskeleton, we propose that mTORC1 controls spindle function during mitosis and meiosis, while mTORC2 contributes to actin-dependent asymmetric division during meiotic maturation in mice.

* Corresponding author:
Laboratory of Animal Reproduction
Graduate School of Agricultural Science
Tohoku University
1-1 Tsutsumidori-Amamiyamachi
Aoba-Ku, Sendai 981-8555, Japan.
E-mail: kogayou8539@gmail.com

Grant sponsor: Japan Society for the Promotion of Science; Grant number: 24248047; Grant sponsor: Grant-in-Aid for Young Scientists (B); Grant number: 21780250

Mol. Reprod. Dev. 80: 334–348, 2013. © *2013 Wiley Periodicals, Inc.*

Received 4 December 2012; Accepted 12 February 2013

Published online 26 March 2013 in Wiley Online Library (wileyonlinelibrary.com).
DOI 10.1002/mrd.22166

INTRODUCTION

Immature mammalian oocytes are arrested at the dictyate stage of the first meiotic prophase, also referred to as the germinal vesicle (GV) stage. A pre-ovulatory stimulus induces the resumption of meiosis, morphologically identified by germinal vesicle breakdown (GVBD), and subsequent events, including chromosomal condensation; alignment of the metaphase-I (MI) spindle and its migration to the cortex; segregation of homologous chromosomes;

Abbreviations: AI, anaphase I; GV[BD], germinal vesicle [breakdown]; MI/II, metaphase I/II; MTOCs, microtubule-organizing centers; mTOR[C], mammalian target of rapamycin [complex]; raptor, regulatory-associated protein of mTOR; rictor, rapamycin-insensitive companion of mTOR; TI, telophase I.

emission of the first polar body; and formation of the metaphase-II (MII) spindle. This process is usually defined as meiotic maturation. In addition to the similarity of morphological steps, the machinery governing female meiotic progression often shares common features with the analogous mitotic process of somatic cells (Solc et al., 2010). In contrast, in the meiotic spindle, alternative mechanisms of spindle assembly and relocation are predominant because oocytes are often devoid of canonical centrosomes and astral microtubules (Szollosi et al., 1972). In mammalian oocytes, microtubule-organizing centers (MTOCs) form the spindle in place of centrosomes (Schatten and Sun, 2009), and the meiotic spindle migrates to the cortex in an actin-dependent manner, rather than requiring astral microtubules (Longo and Chen, 1985; Verlhac et al., 2000; Gonczy, 2008).

The mammalian target of rapamycin (mTOR), an evolutionarily conserved and ubiquitously expressed Ser/Thr protein kinase, forms the catalytic core of at least two functionally distinct complexes, mTOR complex 1 (mTORC1) and mTOR complex 2 (mTORC2). Each complex shares mTOR, mLST8/GβL, and deptor; mTORC1 contains raptor and PRAS40 while mTORC2 contains rictor, mSin1, and PRR5/protor (Bhaskar and Hay, 2007; Jacinto and Lorberg, 2008; Alessi et al., 2009; Cybulski and Hall, 2009; Dunlop and Tee, 2009; Laplante and Sabatini, 2009; Foster and Fingar, 2010). The molecular function of these cofactors remains poorly understood, although the scaffold proteins raptor and rictor have been shown to be required for the downstream effects of their respective complexes, permitting mTOR to bind directly to definite substrates (Kim et al., 2002; Kim and Sabatini, 2004; Wullschleger et al., 2005). Generally, mTORC1 is known to control protein synthesis, cell growth, cell proliferation, and cell cycle progression (Fingar et al., 2002, 2004; Schalm et al., 2003; Fingar and Blenis, 2004; Ruvinsky and Meyuhas, 2006), whereas mTORC2 is associated with control of the organization of the actin cytoskeleton (Jacinto et al., 2004; Sarbassov et al., 2004). In mitotic cells, Ser2448- or Ser2481-phosphorylated mTOR, biomarkers of intrinsic mTOR catalytic activity (Altomare et al., 2004; Lawrence et al., 2004; Yonezawa et al., 2004), and raptor have been shown to exhibit strong expression and have been linked to the localization of the mitotic apparatus (Yaba et al., 2008; Vazquez-Martin et al., 2009a, 2012; Doghman et al., 2010; Lopez-Bonet et al., 2010; Yu et al., 2011). Furthermore, functional studies have demonstrated that mTORC1 is involved in regulation of centrosome number, spindle shape, and chromosome segregation (Bonatti et al., 1998, 2005; Yonezawa et al., 2004; Astrinidis et al., 2006, 2010; Gui et al., 2007; Yu et al., 2011, 2012). Thus, mTORC1 is implicated in mitotic spindle function during the mitotic phase.

Recently, mouse oocyte studies have shown that mTOR mRNA is expressed during oocyte maturation and that mTOR localizes in the nucleus at the GV stage, around the chromosomes at GVBD, and on the spindle at the MII stage. Functional analysis using inhibitor treatment and injection of mTOR antibodies has also revealed that mTOR is involved in GVBD, spindle relocation, and first polar body emission (Yan-Chang and Cai-Rong, 2009; Lee et al., 2012). These reports suggest that, in addition to its roles during mitosis, mTOR participates in many steps of oocyte meiotic maturation, although its detailed roles, particularly focusing on functional variations of each complex, are still unclear. In the present study, we investigated the distribution of mTOR, Ser2448- and Ser2481-phosphorylated mTOR, and components of mTORC1 and mTORC2 during mitosis of cumulus cells versus oocyte maturation in mice in order to compare the distributions and functions of these proteins in mitosis and oocyte meiosis. Here, we report that mTOR and raptor colocalized on the spindle, and phosphorylated mTOR was strongly expressed at spindle poles as well as the midbody in both cumulus cells and oocytes. Rictor was markedly localized around spindle poles only in MI oocytes. These data indicate that mTORC1 may be associated with spindle functions in both mitosis and oocyte maturation, while mTORC2 may control meiotic spindle migration.

RESULTS

Distribution of mTOR and Phosphorylated mTOR in Mouse Cumulus Cells

To examine the distribution of mTOR in mouse cumulus cells, we first performed immunofluorescence staining with antibodies against mTOR and kinase-active Ser2448- and Ser2481-phosphorylated mTOR (pS2448-mTOR and pS2481-mTOR, respectively). In vivo ovulatory stimuli in mice have been reported to induce temporal upregulation of the proliferative capacity of cumulus cells, corresponding to early oocyte meiotic maturation (Hernandez-Gonzalez et al., 2006). Thus, we collected cumulus oocyte complexes 8 hr after culture, the period at which almost all oocytes have progressed to the first meiotic division, in order to obtain cumulus cells in various stages of the cell cycle. Throughout the layer of cumulus cells, mTOR, pS2448-mTOR, and pS2481-mTOR were localized throughout the entire cell (Fig. 1A–I). Notably, when classifying cumulus cells by their nuclear status (Fig. 1A, D, and G), mitotic cumulus cells were also observed in this in vitro maturation system, we observed higher expression levels of pS2448-mTOR and S2481-mTOR in mitotic-phase cells than in other phases of the cell cycle (Fig. 1E–F and H–I).

Intracellular Localization Dynamics of mTOR and Phosphorylated mTOR During Mitotic Progression in Mouse Cumulus Cells

To elucidate the precise distribution of mTOR during mitosis, we followed the intracellular immunolocalization of mTOR, pS2448-mTOR, and pS2481-mTOR during the progression of mitosis in cumulus cells. mTOR, pS2448-mTOR, and pS2481-mTOR were expressed in the cytoplasm at all stages, but the localization of intense expression changed during mitotic progression

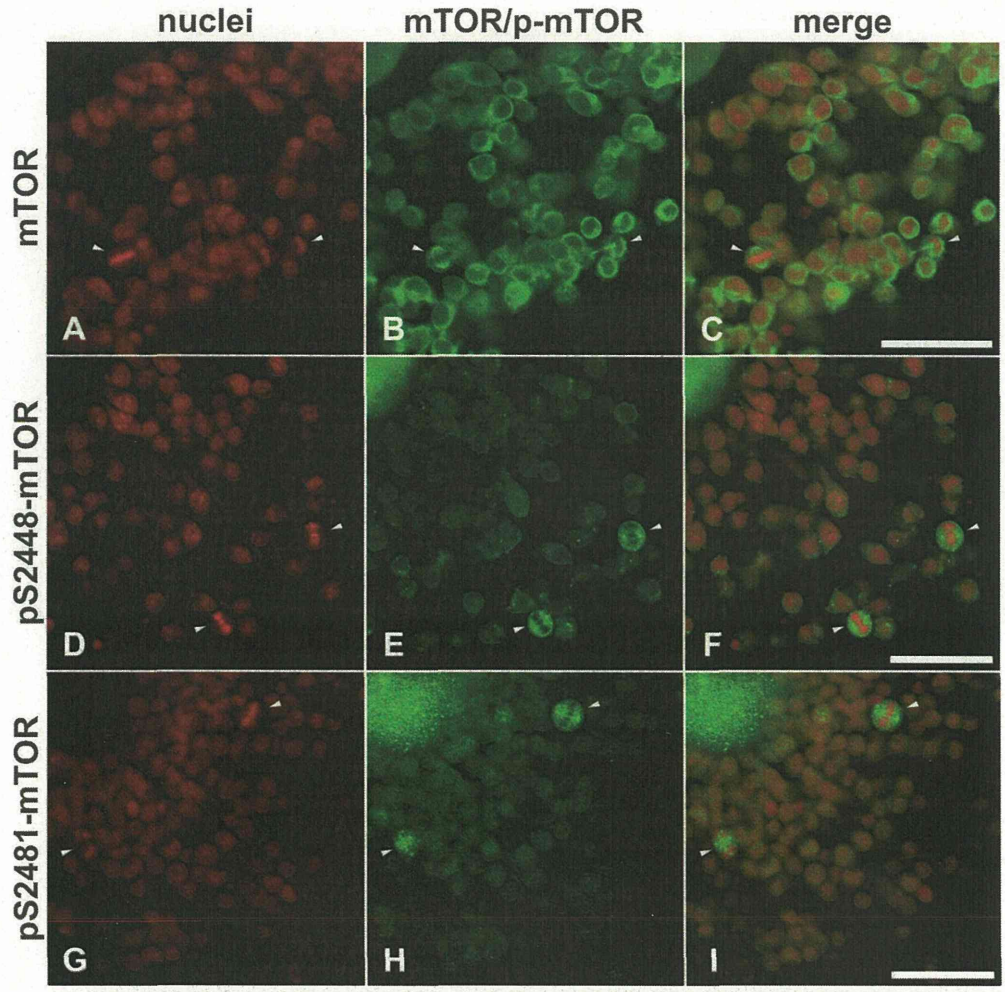

Figure 1. Immunolocalization of mTOR and phosphorylated mTOR in mouse cumulus cells. The panels show nuclei (**A**, **D**, **G**), mTOR or phosphorylated mTOR (p-mTOR; **B**, **E**, **H**), and merged images (**C**, **F**, **I**). Red and green represent nuclei and mTOR/p-mTOR, respectively. The arrowhead indicates mitotic cells. Scale bar, 50 μm.

(Fig. 2Aa–Cf). At interphase, mTOR was distributed mainly in the cytoplasm and subtly in the nucleus (Fig. 2Aa), but was localized principally around the chromosomes at prophase (Fig. 2Ab) and on the spindle between metaphase and cytokinesis (Fig. 2Ac–Af). Both pS2448-mTOR and pS2481-mTOR were distributed in the cytoplasm and in the nucleus at interphase (Fig. 2Ba and Ca), despite the intense speckled pattern localization that was observed adjacent to the chromosomes at prophase (Fig. 2Bb and Cb), on the spindle poles between metaphase and telophase (Fig. 2Bc–Be and Cc–Ce), and on the spindle poles as well as on the midbodies at cytokinesis (Fig. 2Bf and Cf). We observed speckled patterns in the periphery of the cytoplasm for pS2448-mTOR, as shown in the image of telophase (Fig. 2Be). A speckled pattern was observed in the cytoplasm for pS2481-mTOR, including the spindle area (Fig. 2Da–Fd).

Distribution of mTOR, Raptor, and Rictor in Mouse Cumulus Cells

To assess the distribution and colocalization of raptor and rictor with mTOR in mouse cumulus cells, we executed triple staining with antibodies against mTOR, raptor, and rictor. We first confirmed that the same distributions were obtained with triple staining and single staining methods for raptor and rictor (data not shown). Raptor expression and colocalization with mTOR was observed throughout the entire layer of cumulus cells (Fig. 3C and E). Although rictor was also expressed throughout the cumulus cell layer, we

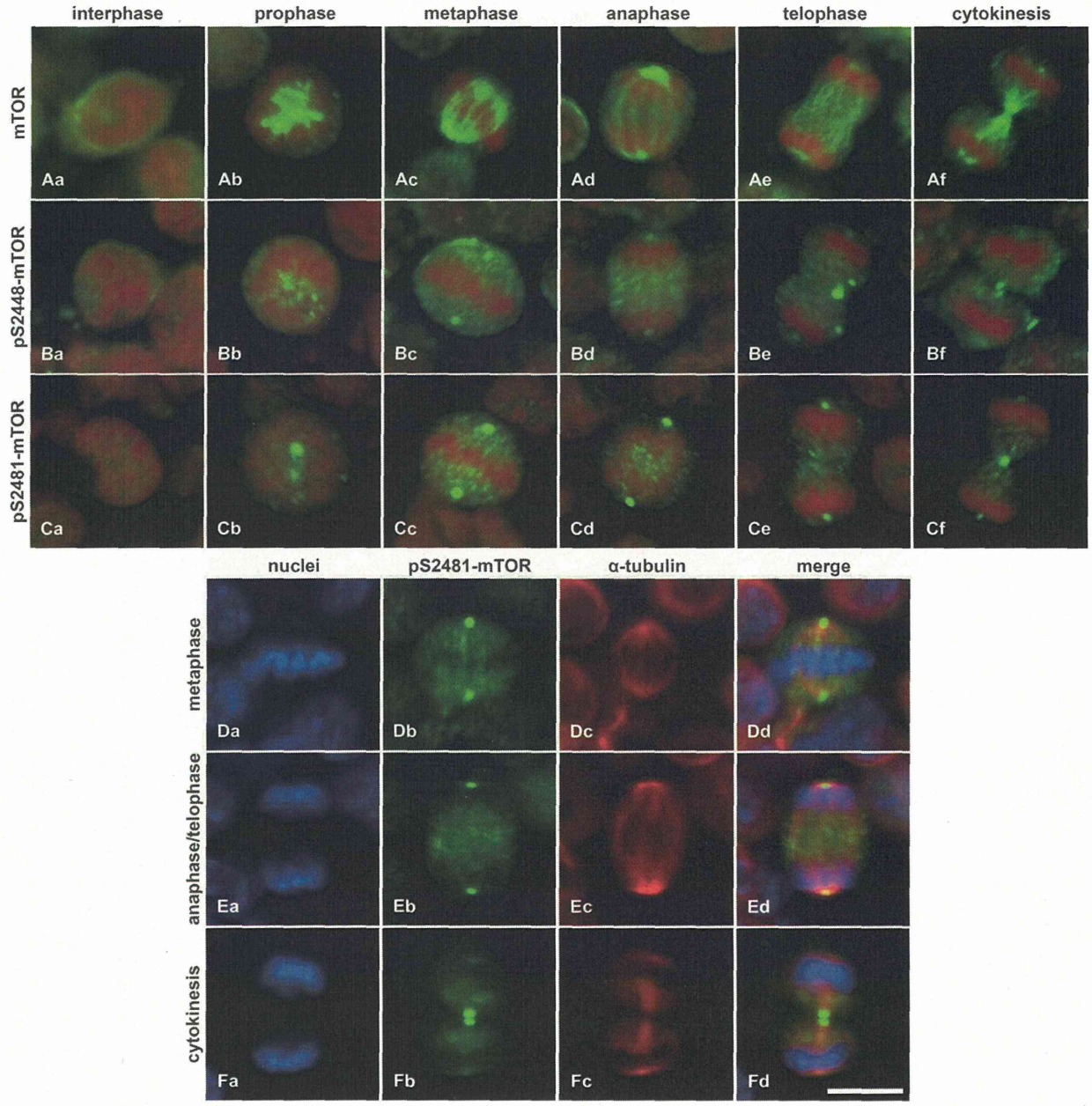

Figure 2. Intracellular localization of mTOR and phosphorylated mTOR at each stage of mitosis in mouse cumulus cells. Panels **Aa–Cf** show mTOR (**Aa–Af**), pS2448-mTOR (**Ba–Bf**), and pS2481-mTOR (**Ca–Cf**) staining, and contain one interphase cell image and five mitotic-phase cell images classified by nuclear status: interphase (**Aa**, **Ba**, **Ca**), prophase (**Ab**, **Bb**, **Cb**), metaphase (**Ac**, **Bc**, **Cc**), anaphase (**Ad**, **Bd**, **Cd**), telophase (**Ae**, **Be**, **Ce**), and cytokinesis (**Af**, **Bf**, **Cf**). Red and green represent nuclei and mTOR/p-mTOR, respectively. Panels **Da–Fd** show nuclei (**Da**, **Ea**, **Fa**), pS2481-mTOR (**Db**, **Eb**, **Fb**), α-tubulin (**Dc**, **Ec**, **Fc**), and merged images (**Dd**, **Ed**, **Fd**), and contain three step-wise mitotic-phase cells including the spindle in metaphase (**Da–Dd**), anaphase/telophase (**Ea–Ed**), and cytokinesis (**Fa–Fd**). Red, green, and blue represent α-tubulin, pS2481-mTOR, and nuclei, respectively. Scale bar, 10 μm.

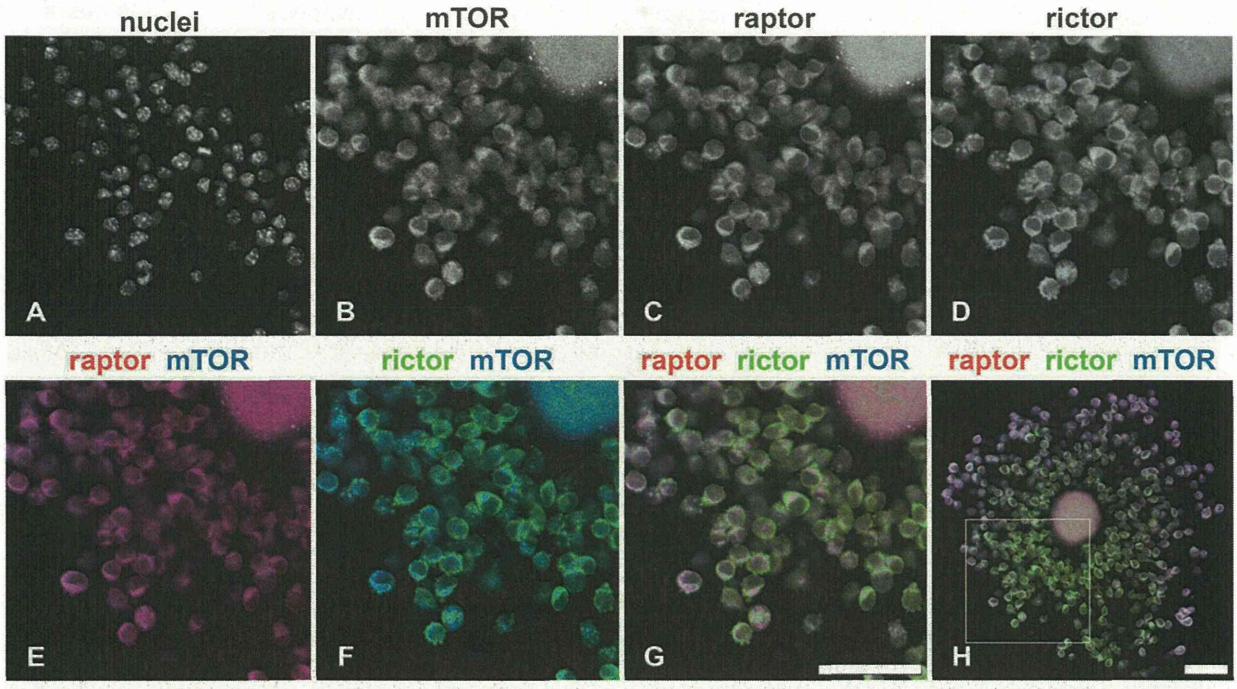

Figure 3. Immunolocalization of mTOR, raptor, and rictor in mouse cumulus cells. The panels show enlarged images of the area surrounded by squares (**A–G**) from the whole cumulus-oocyte complexes (**H**), including nuclei (**A**), mTOR (**B**), raptor (**C**), rictor (**D**), mTOR merged with raptor (**E**), mTOR merged with rictor (**F**), and mTOR merged with raptor and rictor (**G**, **H**). In the merged images, blue, red, and green represent mTOR, raptor, and rictor, respectively. Scale bars, 50 μm.

could not determine definitively whether or not rictor and mTOR exhibited colocalization. In some interphase cells, rictor was dispersed in a punctate pattern (Fig. 3D, F, and G).

Intracellular Localization Dynamics of mTOR, Raptor, and Rictor During Mitosis in Mouse Cumulus Cells

To clarify the distribution and colocalization of raptor and rictor with mTOR during mitosis, we analyzed the subcellular immunolocalization of mTOR, raptor, and rictor during the series of mitotic steps in cumulus cells by the triple staining procedure. Figure 4Ba–Df shows the individual distributions of mTOR, raptor, and rictor, and Figure 4Ea–Gf shows the colocalization of these proteins. Both raptor and rictor were expressed in the cytoplasm at all stages, and subtly in the nucleus at interphase (Fig. 4Ca–Df). Localization of raptor changed during mitotic progression: raptor was distributed in the cytoplasm and the nucleus at interphase (Fig. 4Ca), but was localized predominantly around the chromosomes at prophase (Fig. 4Cb) and on the spindle between metaphase and cytokinesis (Fig. 4Cc–Cf). Additionally, raptor colocalized with mTOR in the cytoplasm and the nucleus at interphase, around the chromosomes at prophase, and on the spindle from metaphase to cytokinesis (Fig. 4Ea–Ef). In contrast, cytoplasmic rictor was localized around, but excluded from, the spindle and did not colocalize with mTOR during mitosis (Fig. 4Da–Df and Fa–Ff).

Distribution of mTOR and Phosphorylated mTOR During Mouse Oocyte Maturation

We next assessed the distribution of mTOR during meiotic maturation using immunofluorescence staining to detect mTOR, pS2448-mTOR, and pS2481-mTOR in mouse oocytes. Oocytes in non-cultured GV, cultured GV, GVBD, MI, anaphase I (AI)/telphase I (TI), and MII stages were, respectively, collected at 0, 4, 6, 10, 12, and 18 hr after culture. The expression of mTOR, pS2448-mTOR, and pS2481-mTOR was confirmed in the cytoplasm at every stage of meiotic maturation (Fig. 5A–U). mTOR was observed exclusively in the cytoplasm in non-cultured GV oocytes (Fig. 5A), but displayed a punctate pattern in the nucleus in cultured GV oocytes (Fig. 5B), intense localization around the chromosomes at GVBD (Fig. 5C), and localization on the spindle during MI–MII stages (Fig. 5D–G). Both pS2448-mTOR and pS2481-mTOR were distributed in a punctate manner in the cytoplasm and nucleus at the non-cultured GV stage (Fig. 5H and O). Meanwhile, they were detected uniformly in the cytoplasm

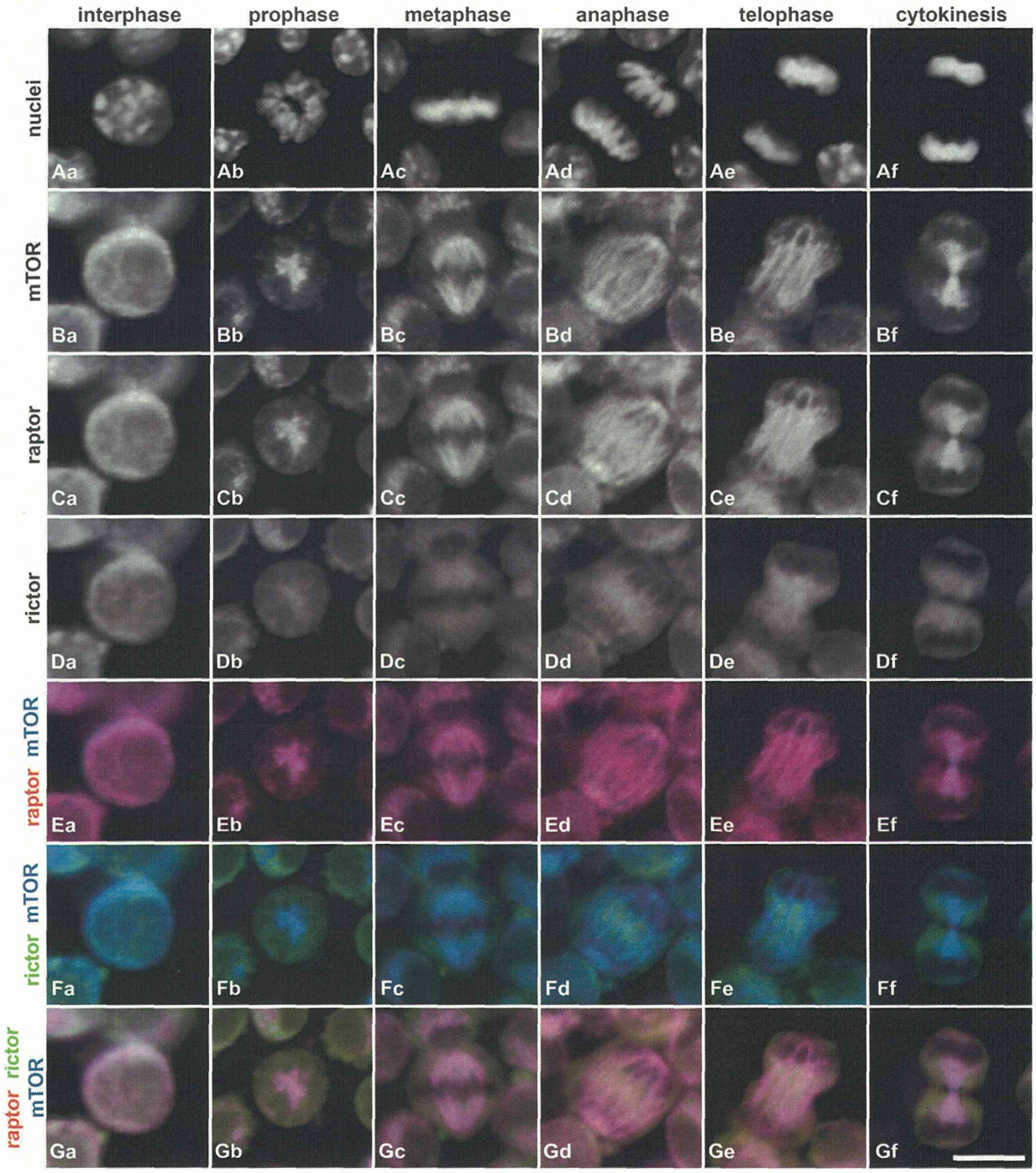

Figure 4. Intracellular localization of mTOR, raptor, and rictor at each stage of mitosis in mouse cumulus cells. The panels show nuclei (**Aa–Af**), mTOR (**Ba–Bf**), raptor (**Ca–Cf**), rictor (**Da–Df**), mTOR merged with raptor (**Ea–Ef**), mTOR merged with rictor (**Fa–Ff**), and mTOR merged with raptor and rictor (**Ga–Gf**), containing one interphase cell image and five mitotic-phase cell images classified by nuclear status: interphase (**Aa**, **Ba**, **Ca**, **Da**, **Ea**, **Fa**, **Ga**), prophase (**Ab**, **Bb**, **Cb**, **Db**, **Eb**, **Fb**, **Gb**), metaphase (**Ac**, **Bc**, **Cc**, **Dc**, **Ec**, **Fc**, **Gc**), anaphase (**Ad**, **Bd**, **Cd**, **Dd**, **Ed**, **Fd**, **Gd**), telophase (**Ae**, **Be**, **Ce**, **De**, **Ee**, **Fe**, **Ge**), and cytokinesis (**Af**, **Bf**, **Cf**, **Df**, **Ef**, **Ff**, **Gf**). In panels **Ea–Gf**, red, green, and blue represent raptor, rictor, and mTOR, respectively. Scale bar, 10 μm.